# An Acoustic System of Sound Acquisition and Image Generation for Frequent and Reliable Lung Function Assessment

Chang Sheng Lee, *Member*, *IEEE*, Minghui Li, *Senior Member, IEEE,* Yaolong Lou, *Senior Member, IEEE*, Qammer H. Abbasi, *Senior Member*, *IEEE*, and Muhammad Imran, *Fellow, IEEE*

***Abstract*— Lung sounds can be translated into acoustic imaging as an alternative to standard imaging to assess lung function frequently for improved therapy efficiency. This study proposes a comprehensive acoustic lung imaging system translated from acquired lung sounds for continual and reliable lung function assessment in response to the growing clinical interest in frequent lung function assessment. The proposed system comprises sub-systems such as data acquisition, signal processing and imaging algorithm. This study demonstrated the design and implementation of a robust lung sound acquisition and imaging system using microelectromechanical microphones that reduce external noise contamination through redesigned hardware and dynamic signal processing. Regarding lung signal acquisition, the proposed system accomplished better root mean square error (RMSE) by around 0.15 and signal-to-noise ratio (SNR) by about 7 dB compared to commercial digital stethoscopes. RMSE and SNR reflect the accuracy in capturing desired signals and robustness to noise contamination and are used to quantitatively compare the system data acquisition to commercially available acoustic and electronic devices in a noisy setting. The proposed system sensors' position is neutral when representing lung signals, with a signal power loss ratio of around 5 dB compared to 10 dB from digital stethoscopes, in terms of sensor sensing sensitivity power spectrum mapping. The proposed system obtains about 7% to 12% more accurate detection of the actual nidus length than digital stethoscopes through imaging translated from acquired lung signals. Additionally, the detected airway obstruction results agree closely (91%) with airway remodeling studies.**

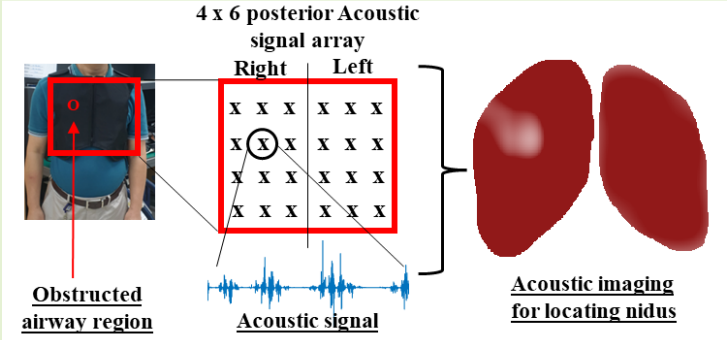


***Index Terms*—Acoustic imaging system, airway obstruction sensing, biomedical acoustics sensor, lung sound signals, MEMS microphone.**

This Manuscript submitted XXX XX, 2023. This work was supported and funded by the Singapore Economic Development Board (EDB).

Chang Sheng Lee is with the James Watt School of Engineering, University of Glasgow, Glasgow G12 8QQ, United Kingdom, and with Global Technology Integration department, Hill-Rom Services Pte Ltd, 1 Yishun Ave 7 Singapore 768923 (e-mail: LeeChangSheng@outlook.com).

Minghui Li is with the James Watt School of Engineering, University of Glasgow, Glasgow G12 8QQ, United Kingdom (e-mail: David.Li@glasgow.ac.uk).

Yaolong Lou is with the Global Technology Integration department, Hill-Rom Services Pte Ltd, 1 Yishun Ave 7 Singapore 768923 (e-mail: yllou@ieee.org).

Qammer H. Abbasi is with the James Watt School of Engineering, University of Glasgow, Glasgow G12 8QQ, United Kingdom (e-mail: Qammer.Abbasi@glasgow.ac.uk).

Muhammad Imran is with the James Watt School of Engineering, University of Glasgow, Glasgow G12 8QQ, United Kingdom (e-mail: Muhammad.Imran@glasgow.ac.uk).

## I. Introduction

Chest X-rays or Computed Tomography (CT) are usually used during periodical medical visits to check the patient's lung function. As a result, adapting medical therapy to each patient's unique medical progression is challenging. The therapy result may be strengthened by frequent or continuous observation of lung functions throughout the patient's everyday tasks [1], [2].

An uncomplicated technique for frequent lung function assessment is acoustic imaging. Acoustic imaging may enhance healthcare delivery to patients with lung diseases, resulting in early detection of the condition worsening, adjusting to the therapy and achieving a higher quality of life, and decreased hospitalization rates [3], [4]. Thus, a need has arisen for portable devices with acceptable accuracy, cost, and simple setup to monitor essential parameters such as locating airway obstructions (nidus) and tidal volume changes over time.

Acoustic imaging systems such as vibration response imaging (VRI) [5]–[7] employ an array of digital stethoscopes alike, recording the respiratory signals and converting the multiple signals from the array of digital stethoscopes to acoustic images for lung function assessment [7]. The visual representation enhances clinical relevance by providing localized data on breath sounds between various lung locations [5]–[7]. Although there is a positive quantitative data link between VRI and lung problems, such as smoking index and the buildup of excess fluid between layers of the pleura outside the lungs [5]–[7], there is no positive data correlation in locating obstructed airways (nidus) between VRI and airway-related diseases, such as asthma and COPD [5]. Hence, biometric sensors, such as digital stethoscopes used for capturing lung sound and later converting to acoustic images for lung function assessment, still need to be developed significantly [7], [8]. Additionally, studies in [8] and [9] find no accurate, noninvasive, affordable, or simple-to-use biometric sensor to measure changes in the airways. An accurate data representative, such as acoustic lung signals and images of the patient's lung function, is vital in this study. Therefore, designing a portable, low-cost, and efficient lung sound acquisition platform is needed for reliable lung function assessment via acoustic lung imaging.

In this paper, a wearable acoustic lung imaging system translated from reliable lung signals is proposed. To the best of our knowledge, the proposed system, presented in Fig. 1, comprises various sensing and functional components, including an onboard computer and an array of daisy-chained microelectromechanical systems (MEMS) microphones (see Fig. 1(b)) packaged into a standalone or wearable mobile device for the assessment of lung function via acoustic imaging translated from lung sounds captured from the array of MEMS microphones have not been investigated. The suggested system is straightforward to operate, and no specialized training is required to interpret the assessment results. The suggested system has the flexibility in implementing the array of MEMS microphone, e.g., the number of sensors required and the sensor position. A denoising algorithm [10] specifically created to enhance captured lung sounds by actively suppressing unwanted interfering noise from the environment, including noises with a spectral signature that coincide with the body sounds, is integrated into the proposed system (see Fig. 1(c)) and has outperformed commercial digital stethoscopes, such as Thinklabs One [11] and Littmann 3200 [12], in terms of root mean square error (RMSE) by about 0.15 and signal-to-noise ratio (SNR) by around 7 dB. Thinklabs One [11] and Littmann 3200 [12] were selected as a benchmark in this study due to their filtering capabilities and improved ability to acquire acoustic signals. The SNR describes the signal quality and strength with respect to the environment noise while maintaining the lung signal frequency of interest, while RMSE findings show the system's ability to retain critical characteristics of lung sound post-signal processing. Compared to the commercial digital stethoscopes, the loss ratio for our hardware system is around 5 dB compared to about 10 dB in terms of the sensor area sensing sensitivity power spectral mapping, so the quality of signals collected is less sensitive by the position of the sensor on the chest area. In terms of sensor-detecting sensitivity mapping, the microphone array maximizes measurement sensitivity and uniformity.

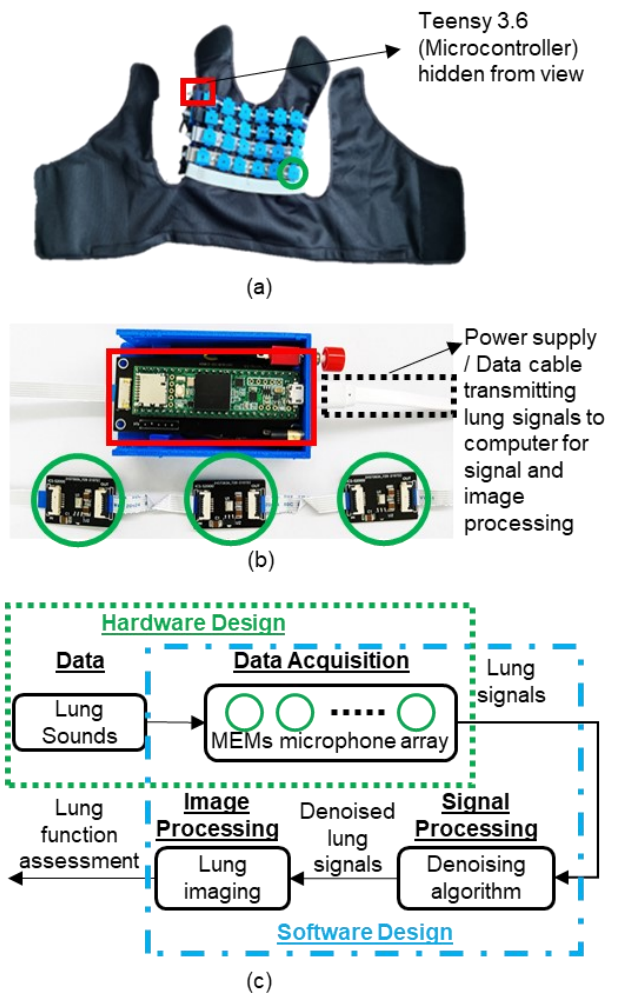


Fig. 1. The overview of the proposed acoustic imaging system for self-assessment of lung function. (a) An array of wearable MEMS sensors denoted as ○ for simultaneous acoustic lung signal acquisition interconnected with flexible printed circuit cable. (b) Sub-system data acquisition and control unit consisting of a microcontroller and daisy-chained multimicrophone array (without cover). (c) The data flow and the acoustic imaging sub-system.

An experimental study on identifying airway blockage via imaging was carried out using the proposed system, and the results were supported and correlated by the sensor distribution and acoustic imaging resolution findings in [13] and [14]. Waterbags with various diameter sizes between 50 mm and 80 mm were placed on the posterior of a healthy volunteer to mimic the airway obstruction, akin to the literature [15]–[17], to illustrate the effect of presenting accurately obstructed lung images from captured lung sounds. Multichannel respiratory signals were captured with the proposed system, equipped with an array of MEMS microphones with the array design recommendation from [13], [14], and the imaging output translated from lung signals from our system and commercial digital stethoscopes were analyzed [13], [14]. Our system is about 7 to 12% more accurate in detecting airway obstruction as compared to commercial digital stethoscopes through acoustic imaging translated from the captured lung signal. Hence, capturing accurate acoustic signals is critical in determining lung function. Furthermore, the identified airway

obstruction with our hardware system correlates closely (91%) to the modeling and simulation design work in [13] and [14]. The proposed acoustic imaging system can be used for various potential purposes, including home-based screening for respiratory disorders by clinicians located elsewhere than the patients, gating controls for radiological imaging procedures, and reducing infection concerns associated with intra-hospital patient transportation to the equipment and lower machine operating expenses [3], [4], [18], [19].

This paper is organized as follows: A concise literature review on lung function assessment is described in Section II. The hardware data acquisition and the design setup are presented in Section III. The performance index and setup of the proposed system signal acquisition in relation to noise, and the accuracy of acoustic imaging are presented in Section IV. The experimental results and discussion are presented in Section V. Lastly, Section VI presents the conclusion and future work.

## II. Literature Review

Although chest X-rays and CT are dubbed as the gold standard technique for lung function assessment due to their accuracy and reliability method, it is time-consuming, expensive (> USD 5000) and complicated to operate, and can only be performed in medical settings (patient-to-equipment approach) [7], [8]. Moreover, chest X-rays and CT require medically trained personnel to interpret the assessment results and expose patients to harmful radiation, making frequent lung function assessments impractical.

Acoustic imaging through analysis of the captured acoustic signal from an array of sensors at multiple locations is an alternative for lung function assessment and has an equipment-to-patient approach, particularly for cases where the patient's movement is restricted or discouraged due to disabilities, pandemic, or inaccessibility to facilities rendering traditional techniques unfavorable. Acoustic signals and imaging providing intuitive assessment results have been proposed as a potential means for frequent monitoring and early assessment of lung function [7], [8], [15], [16], [20], [21]. Feasibility studies [13], [14] were performed on acoustic signals and imaging for detecting and locating airway obstruction via remodeling and simulation. The lung disorders' location and severity can be identified via acoustic imaging transmuted from the captured lung sounds via an array of digital sensors at different locations [6], [8], [13], [15], [16], [20], [21]. Capturing robust acoustic signals produced from the patient's chest wall is critical for assessing lung function via acoustic imaging.

In the quantitative forms of acoustic signal representation, VRI employs an array of digital stethoscopes alike, records the vibration energy generated during breathing, and converts the breath sounds to an image for lung function assessment [5]–[7]. Digital stethoscopes such as the Thinklabs One [11] and Littmann 3200 [12] are a few examples developed with filtering capability for computerized analysis and signal quality enhancement to eliminate subjectivity in interpreting results, unpredictability, and inconsistency between listeners and susceptibility to airborne ambient noise. However, these systems are still susceptible to dynamic noise in most real-world settings [9] and are expensive (> USD 300) [11], [12] as a single unit. Background conversation and other environmental disturbances are frequent in many settings, and patient movement taints the sound signal captured by the stethoscope. The denoising function becomes critical in lung-sound signal processing, as the captured lung sounds can affect the acoustic imaging assessment. An additional vacuum seal is required for the VRI digital stethoscopes sensor alike to achieve proper contact with the patient's body, making the device interfering and impractical to integrate with other body sensor networks or respiratory therapy devices for frequent home-based monitoring. Furthermore, remote monitoring or home-based assessment through digital stethoscopes requires advanced patient compliance and position accuracy.

## III. System Design

Fig. 2 depicts the workflow for the system's acquisition of acoustic signals through an array of MEMS microphones and ends with acoustic lung images converted from lung sounds. Compactness, dependability, and usability were the three design priorities for the hardware. Our distinctive programmable system illustrated in Fig. 2's block diagram consists of an array of MEM microphones and was designed to address two known limitations with digital stethoscopes: 1) robustness in noisy environments; and 2) accurate acoustic imaging representation. The MEMS microphone module captures the acoustic signals originating from the air hitting the airway wall (airflow) and converts the airflow to acoustic (electrical) signals, which can then be communicated to the microcontroller as digital data. Sections III-A and III-B, respectively, each describe the hardware and software system design.

### A. Hardware Design

The following sub-sections discuss the hardware components utilized for the proposed system, the data acquisition module, and the design of the acoustic sensor array, as shown in Fig. 1(c).

#### 1) *Hardware Components*

A digital time-division multiplexing (TDM) and daisy chained enabled ICS-52000 (TDK, USA) [22] output bottom port microphone was utilized in our system design to capture lung sound. The ICS-52000 was soldered onto a printed circuit board (PCB), as shown in (Fig. 3), with a voltage regulator consisting of a ferrite bead and two (2) capacitors denote as C1 in Fig. 3(b). The ICS-52000 features a broad frequency response from 50 Hz to 20 kHz, covering the typical lung sound

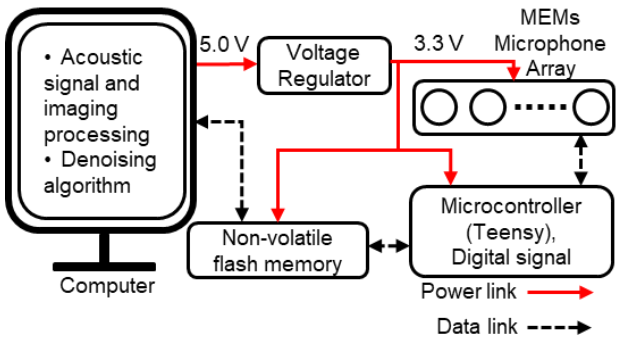


Fig. 2. The overview block diagram of the system setup.

This article has been accepted for publication in IEEE Sensors Journal. This is the author's version which has not been fully edited and content may change prior to final publication. Citation information: DOI 10.1109/JSEN.2023.3344136



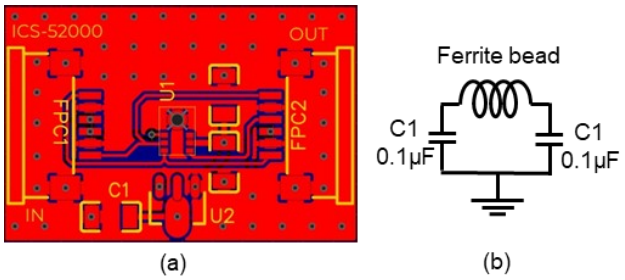


Fig. 3. (a) PCB design for ICS-52000 and its electrical components and connections, where U1 represents ICS-52000, and FPC denotes flexible printed circuit cables to transmit the data from U1 to the microcontroller. (b) The voltage regulator connection for ICS-52000 is represented as U2.

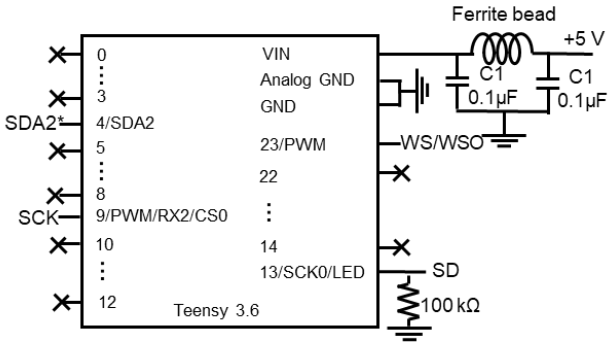


Fig. 4. Digital pins utilized on Teensy 3.6 board for this study. Digital pin 4 is only required when multiple Teensy 3.6 board is required (see Fig. 7). For other digital pins usage and details, refer to [26].

frequency range [15], [16], [23], [24]. Digital TDM microphone was selected as the 24-bit industry-standard TDM interface enables an array of up to 16 ICS-52000 microphones to be daisy chained to a single digital signal processor, and without the use of an audio codec in the system — reducing the number of physical components and computation power. The MEMS microphone's characteristics were selected so that its lung signal acquisition capabilities are comparable to those of a commercial digital stethoscope [8], [11], [12], [16], [20], [25].

Teensy 3.6 (PJRC, USA), a 32-bit, 180 MHz ARM Cortex-M4 core equipped, was selected as the microcontroller for the MEMS microphone due to the compact design that can be easily integrated into a wearable device, and it is an all-inclusive processor configurated for a customized solution that offers flexibility in programming, adjusting parameters, and updating algorithms. A digital signal processing solution is chosen in our system design as it is programmable so that the signal processing parameters can be individualized. The Teensy 3.6 board assembly for the system hardware design is presented in Fig. 4, where Teensy 3.6 was soldered to a PCB for stability that has a voltage regulator converting 5 V to 3.3 V supplied to the MEMS microphones, and a 100 kΩ pulldown resistor at the serial data (SD) output to discharge the output line during the microphones' three-state logic on the data bus.

### 2) *Data Acquisition System Design*

The word select (WS) signal synchronizes ICS-52000 microphones, ensuring that acoustic signals recorded from several microphones using the same clock will be sampled simultaneously. A delay to the start of the frame sync WS signal is implanted to the ICS-52000 MEMS microphone sensor by enabling WS output on the clock master by 512 ms after the serial clock (SCK) is activated. The delay allows the internal circuits of the microphone to initialize properly before beginning the synchronization sequence with other microphones in the TDM array. Fig. 5 demonstrates an example of an array of MEMS microphones connected on a single data bus, in which the slave serial data port's format is TDM.

The WS clock master from the microcontroller drives the WS signal of the first MEMS microphone. The array of MEMS microphones was daisy-chained, allowing the first MEMS microphone WS output (WSO) to drive the WS of the second MEMS microphone, etc. The first TDM slot will be used to output data from the ICS-52000, the second TDM slot will be used to output data from the next microphone in the chain, etc. The word length output data is 24 bits/channel, and the data word format is the most significant bit first and 2's complement. The frequency of SCK utilized in our system design employing

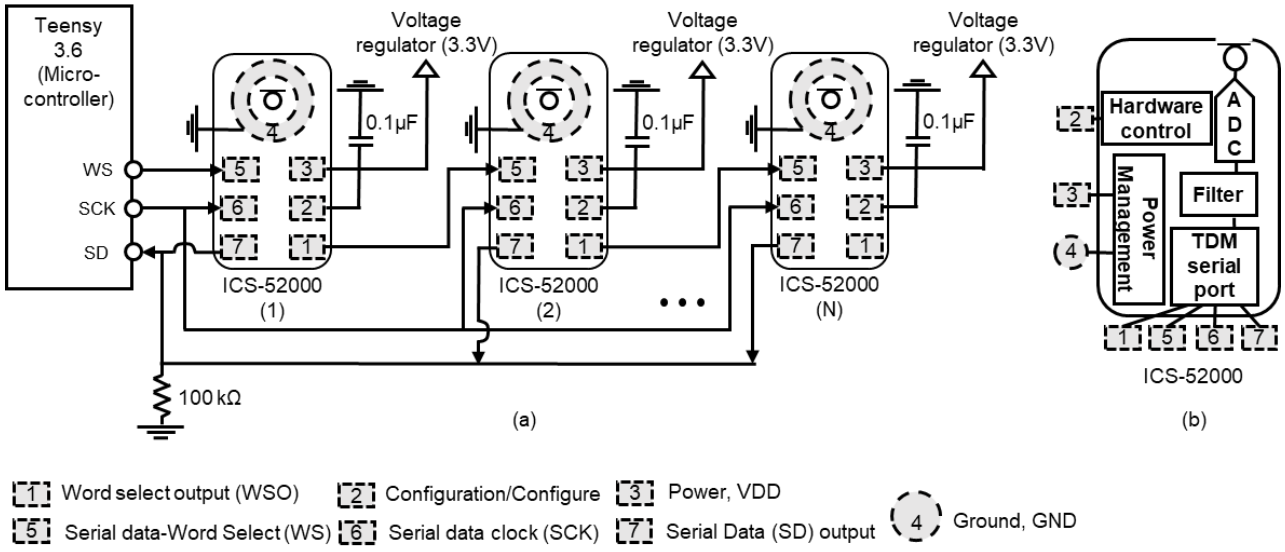


Fig. 5. Overview of the connections between daisy-chained MEMS microphone and microcontroller. (a) System block diagram of digital pin connections for an array of MEMS microphones. (b) ICS-52000 digital pin and its modules.

This article has been accepted for publication in IEEE Sensors Journal. This is the author's version which has not been fully edited and
content may change prior to final publication. Citation information: DOI 10.1109/JSEN.2023.3344136



5–8 MEMS microphones in a chain is given as 256 × $f_{WS}$, where WS frequency ($f_{WS}$) is about 8000 Hz [22].

The design of an array of microphones can assess lung function via acoustic imaging, translated from the multichannel lung sound signals, similar to VRI [20], [21] and studies in [13] and [14]. From Fig. 5, the ICS-52000 package incorporates a MEMS microphone sensor with a sensitivity tolerance of ±1 dB, allowing high-performance microphone arrays and eliminating the requirement for system calibration; signal conditioning, such as digital filter removing unwanted low-frequency noise from the direct current and synchronized sampling of all microphones in an array of acoustic signals enabling accurate array processing; an analog-to-digital converter; decimation and anti-aliasing filters; and power management.

3) *MEMS Microphone Array Design*

The practicality of designing an acoustic imaging system regarding the number of sensors and sensor sensing diameter needed to achieve the desired minimum detectable obstructed airway (nidus length) is shown in Fig. 6 [13], [14]. With more sensors, the detectable minimal nidus length could be resolved more precisely due to the larger overlap of the sensor sensitivity area, e.g., with the same sensing diameter of 50 mm, a detected nidi length of 73 mm requires about 4 sensors and nidi length of 25 mm requires about 24 sensors on one side of the chest.

As up to 16 ICS-52000 can be daisy chained in an array with one microcontroller, Fig. 7 demonstrates an array of Teensy 3.6 board connections for an acoustic signal acquisition system or acoustic imaging system [6], [7], [15], [17], [20], [21] requiring more than 16 MEMS microphones [13], [14]. 1 microcontroller is utilized for up to 8 daisy-chained MEMS microphones in our paper.

The Teensy 3.6 and ICS 52000 MEMS microphones connections are demonstrated in Fig. 4, Fig. 5, and Fig. 7. Flexible printed circuit (FPC) connectors and cables were utilized to connect Teensy 3.6 to the external microphones due to its lightweight interconnection enabling the system wearability, as illustrated in Fig. 1, and Fig. 3. The standard USB type A-USB micro interface was utilized to transfer

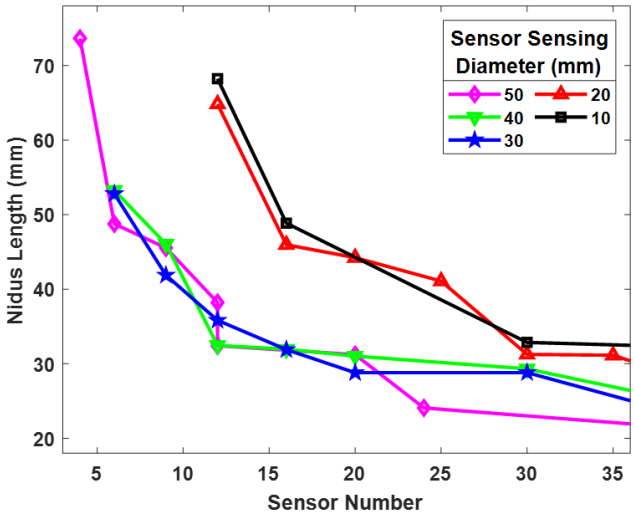


Fig. 6. The typical sensor numbers in a practical acoustic imaging system that can be observed on one side (right posterior) of the chest wall.

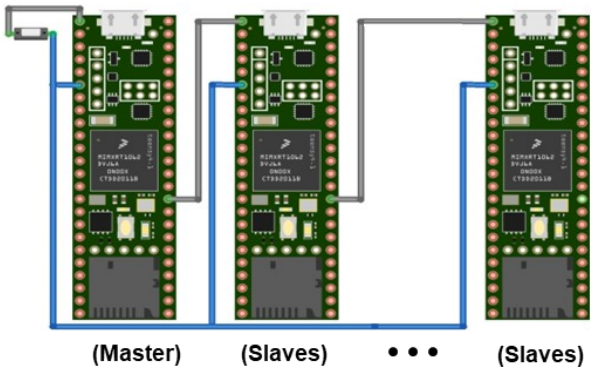


Fig. 7. Teensy 3.6 boards connection for multiple arrays of a maximum of 16 MEMS microphones each, with the first Teensy 3.6 board as a control (master) with a master switch, and the subsequent Teensy 3.6 boards as slaves. Grey represents the ground connection, and blue represents the interconnection of digital pin 4 (SDA2).

MEMS microphones data to the memory card 115,200 bit/s baud rate and then to the computer for digital acoustic signal analysis. Arduino sketchbook v1.8.13 was used as the programming software activating Teensy 3.6 microcontroller in acquiring acoustic signals through the array of MEMs microphones. Real-time computerized lung sound analysis, adjustments to digital signal processing, and usability improvements can all be implemented on the same hardware platform owing to the flexibility of the programmability.

## B. Software Design

The following sub-sections illustrate the software data acquisition module, signal processing module and acoustic lung image processing from the acquired lung signal, as presented in Fig. 1(c).

1) *Data Acquisition Software Design*

The overall block diagram of software design, including the data acquisition module, is illustrated in Fig. 8. Through the connected serial port, the microcontroller waits for the computer to send a data transmission command to collect acoustic signals via MEMS microphones. The collected data is then stored in the non-volatile flash memory when the acoustic signals from the MEMS microphones come in. The collected digital data is saved in XLS format with separate columns according to the individual MEMS microphone digital data in

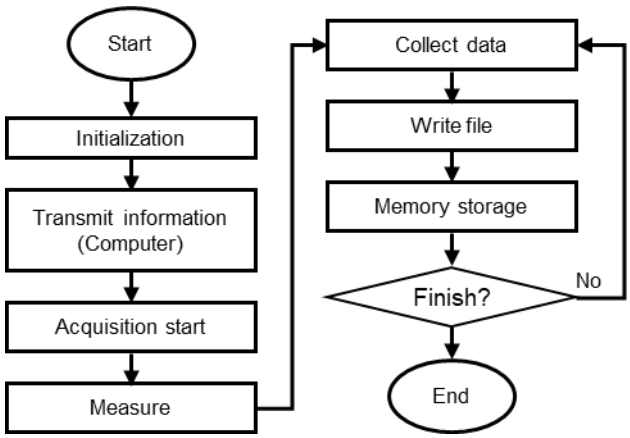


Fig. 8. Software overall flowchart for the acquisition of acoustic signals.

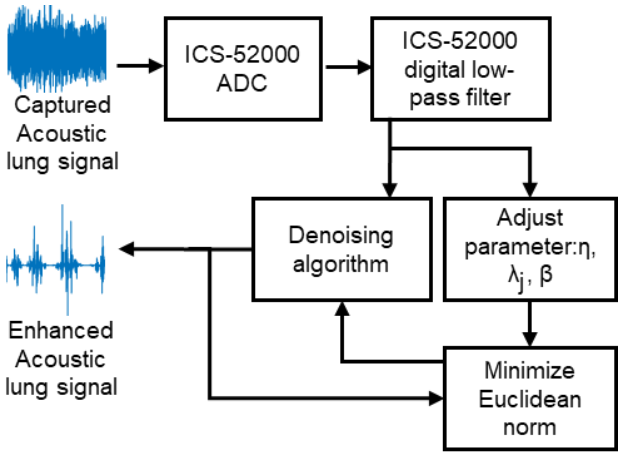


Fig. 9. Software flowchart for signal collection and integrated post-processing denoising.

an array.

2) *Signal Processing Denoising Module*

Fig. 9 shows the proposed system's input and output flow of the acoustic signal. The input signal sampling frequency $F_S$ of the system is 8000 Hz. From Fig. 9, an ICS-52000 in-built digital low pass filter [22], and denoising algorithm [10] are applied to suppress the inference, such as ambient- and patient-generated noise to enhance the acquired lung signal through MATLAB R2023a.

The ICS-52000 in-built filter's lower cutoff frequency is set to 50 Hz, and the upper cutoff frequencies extend to $0.417 \times F_S$ and 0.04 dB ripple within the pass band, according to the datasheet [22]. E.g., the sampling frequency $F_S$ of 8000 Hz utilized in this paper results in a bandpass frequency response from about 50 Hz to 3336 Hz [22]. The in-built filter was utilized to eliminate high-frequency noise as the ICS-52000 uses a single-bit, high order, sigma-delta analog-to-digital converter (ADC) that operates at a high oversampling ratio [22]. The in-built filter characteristics scale with sampling frequency.

Delivering denoised signals from ambient noise while carefully avoiding the cancellation of auscultation patterns that are indicative of diseases, such as crackling that can easily pass for noise, is one of the primary concerns of implementing denoising in acoustic lung sound recording systems. The simple addition of an active noise-canceling filter or typical finite impulse response filter [8], [10], [27] to an acoustic MEMs microphone does not adequately solve these concerns [24]. Hence, a novel denoising method [10] is included in our system design, as shown in Fig. 2 and Fig. 9, which is based on wavelet transformation that are used in the fields of lung sound signals denoising [10], [24], [27]. This approach is optimum for removing external noise while retaining the desired signal. An empirical Wiener filter and a unified wavelet threshold denoising filter (WATV) are combined in the approach. The algorithm has been validated and given in-depth details before in [10] and has been tested on actual lung sound signals collected from patients with respiratory disorders in a noisy clinical environment. A summary of the denoising filter approach and the implementation is summarized below.

The captured signal $y(n)$ from the sensor contains the desired signal $x_a(n)$ and noise $v(n)$ such as the ambient noise, and the inherent noise from electronic devices as shown in (1),

$$y(n) = x_a(n) + v(n), \tag{1}$$

where $n$ is the sample index $n = 1, 2, 3, \ldots, N$, and the total number of samples $N$ is given as $N = F_S T$, where $F_S$ is the sampling frequency, and $T$ is time.

Before attempting to achieve a sufficient denoised signal coefficient from the lung sounds, WATV is first utilized to lessen the interference noise, achieving adequate denoised signal coefficients by adjusting a control parameter $0.95 \leq \eta < 1$. The control parameter $\eta$ influences the total variation parts $\beta$ and the regularization parameter $\lambda_j$ , where $\beta$ and $\lambda_j$ control the pilot estimation of the denoised wavelet coefficients in the denoising algorithm [10]. Following the pilot estimation, the estimated signal coefficient is sent into the empirical Wiener filter for smoothing by minimizing the denoised signal overall mean square error through inverse filtering. The pseudocode of the denoising algorithm is presented below.

**Algorithm 1. WATV-Wiener denoising algorithm**

**Input:** Noisy data ($y$); Number of vanishing moment ($k_m$); Regularisation parameter ($\lambda_j$); TV parts ($\beta$); Step size ($\mu$); Number of wavelet scale ($j$); Number of iterations ($niter$); Threshold function ($\theta$); Wavelet transform (W); Wavelet coefficient ($\omega_c$)

**Output:**

Initialisation: $\omega_c = \mathrm{W}y$;
Identifying wavelet coefficient in (4.10) by iteratively minimising with respect to $\omega_c$ and $u$ with variable splitting and augmented Lagrangian approach.
$u = \omega_c$; $d = \omega_c$; $c = 0$;
Iteration till convergence between $\boldsymbol{\omega_c}$ and $\boldsymbol{u}$.
**For** $i = 1{:}niter$
$p_{j,k} = [\mathrm{W}y + \mu(u - d)]/(1 + \mu)$
Finding the wavelet coefficient $\omega_c$ for all $j, k_m$ with the input from $\theta$, $p$, $\lambda_j$, $\mu$, $a_j = 1/\lambda_j$
$\omega_{c(j,k)} = \theta\left(p_{j,k}; \lambda_j/(1 + \mu); a_j\right)$
$c = d + \omega_c$
Total variation denoising ($tvd$) requires data input from $c$, length of the data input ($N$) and TV parts
$d = \mathrm{W}[\mathrm{W}^{-1}v_t - tvd(W^{-1}c; N; \beta/\mu)]$
$u = c - d$
$d = d - (u - \omega_c)$
**end For**
Denoised wavelet coefficient ($\hat{\omega}_c$), where the signal $\hat{x}_t = \mathrm{W}^{-1}\hat{\omega}$
Empirical Wiener filter design for smoothing: $H$
$H = \hat{\omega}_c{}^2/\left(\hat{\omega}_c{}^2 + \sigma^2\right)$
Smooth denoised output: $\hat{x}_a = \mathrm{W}^{-1}H\mathrm{W}\hat{x}_t$

3) *Image Processing*

Using an image processing approach [13], [14], [21], the acquired lung signals are transformed into acoustic images for analysis in MATLAB 2023a. The lung signal intensity $\bar{P}$ at each sensor location $i$ in a $x$- and $y$-axis coordinate plane is computed by accumulating the acquired signals $P$ over a known time $t$ interval from $t_1$ to $t_k$,

$$\bar{P}\left(x,y,t_1,t_k\right)=\sum_{t=t_1}^{t_k}P_i(t)^2 \tag{2}$$

The acoustic lung imaging $Q$ projected from lung signals is then,

$$Q\left(\bar{P},h\right)=\sum_{t=t_1}^{t_k}P_i(t)^2\,h\left(j\right). \tag{3}$$

where $Q(\bar{P}, h)$ comprises of acoustic signal $\bar{P}(x, y, t_1, t_k)$ and interpolation function $h(j)$, with $j$ containing the intensity output from $\bar{P}(x, y, t_1, t_k)$ with the sensor position $(x, y)$ information. Hermite interpolation polynomial is applied to estimate sound intensity outside of the sensor position on the chest area [5], as high spatial resolution is required for the limited number of sensors that can be placed onto the chest wall [17] and is given as,

$$h\left(j\right)=\sum_{s=0}^{d}\left(h_s-2L_s'(j_s)(j-j_s)L_s^{\,2}(j)h_s+(j-j_s)L_s^{\,2}(j)h_s'\right), \tag{4}$$

where the prime ($'$) symbol refers to the derivative function, $d$ is the degree of the polynomial, and $L$ is the Lagrange polynomial with the known pixel locations $m$ given as,

$$L_s\left(j\right)\triangleq\prod_{s=0,s\neq m}^{d}\frac{j-j_s}{j_m-j_s}. \tag{5}$$

Refer to [17] for the Hermite interpolation function in-depth analysis, computation, and application on acoustic lung imaging. The highest, lowest, and in-between values are determined as maroon, white, and grey.

Fig. 10(a)–Fig. 10(c) present the time-domain digital amplitude of the three sensors, showing the respiratory breathing phase as observed in terms of waveform peak and valley. Fig. 10(d) present the frequency spectrum of the three devices, where the frequency of interest is in a similar range centered around 220 Hz and is within the typical frequency of lung sound signals [8]. The ICS-52000 MEMS microphone outputs digital amplitude using its internal proprietary ADC [22], similar to the two commercial digital stethoscopes. All three sensors, MEMS microphone, Thinklabs One, and Littmann 3200 output unitless digital amplitude. Each acoustic signal $\bar{P}(x, y, t_1, t_k)$ captured from the single data point is put into an array (matrix) form in MATLAB R2023a, the array of acoustic signals is normalized, and acoustic images are then displayed as the output collected from the intensity (digital amplitude) of the sound signal. A cone-shaped lung mask image processing, was applied to enhance the acoustic image output in (3) for better aesthetic visualization to the end-users, similar to acoustic imaging studies in the literature [5], [6], [8], [15], [21].

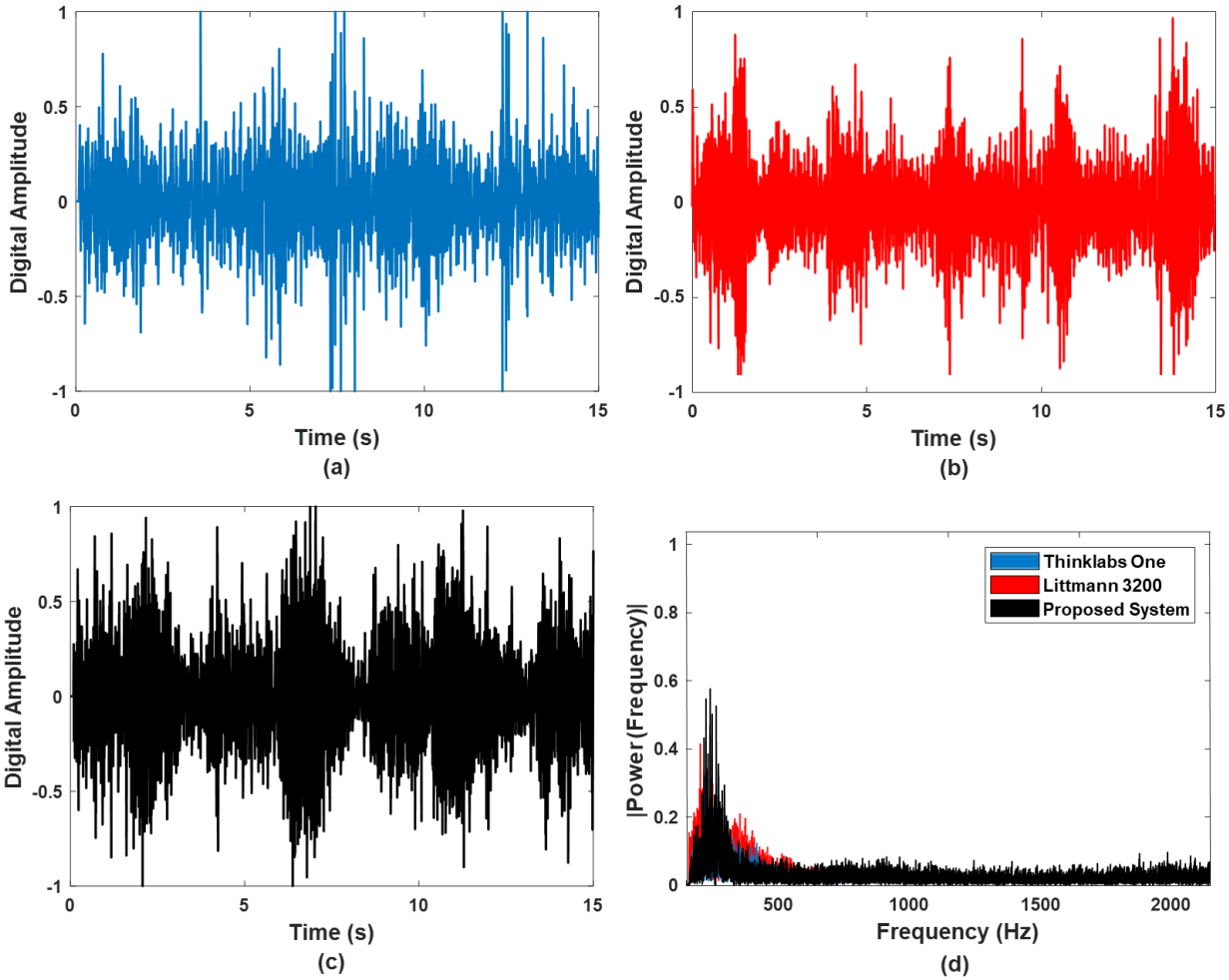


Fig. 10. Recorded digital amplitude relation to the respiratory sound signals and the frequency spectrum of the recorded lung signals. (a) Thinklabs One time-domain respiratory signals output, (b) Littmann 3200 time-domain respiratory signals output, (c) Proposed system time-domain respiratory signals output and (d) the frequency of interest for the three devices.

## IV. System Performance Evaluation

In terms of acquiring robust and accurate lung signals, our system's lung signal acquisition unit is compared with commercially available digital stethoscopes, Littmann 3200, and Thinklabs One, which are integrated with cutting-edge denoising technologies to precisely measure the system design standards [11], [12]. Littmann 3200 and Thinklabs One digital stethoscopes were selected due to their unique design and setting that impact the transmitted sound's characteristics and improve acoustic signal collection performance [11], [12]. The homogeneity of the transducing mechanism, quality preservation of transmitted lung sounds, and robustness to unwanted ambient noise are three critical factors in measuring the system's performance. Hence, RMSE, SNR, and sensing sensitivity are crucial performance indicators for measuring how well sensors capture accurate lung sound signals in relation to noise.

A concise experimental verification was performed to identify airway obstruction and the findings in the airway remodeling and simulation studies [13], [14]. All system performance analyses and results were performed in MATLAB R2023a. The lung sound acquisition and imaging setup are described in Section IV-A. Sections IV-B covers the performance index of the sub-system data acquisition, such as the sensor sensing sensitivity, acquired signals quality, and identification of nidi through imaging translated from the acquired lung signals.

(a)

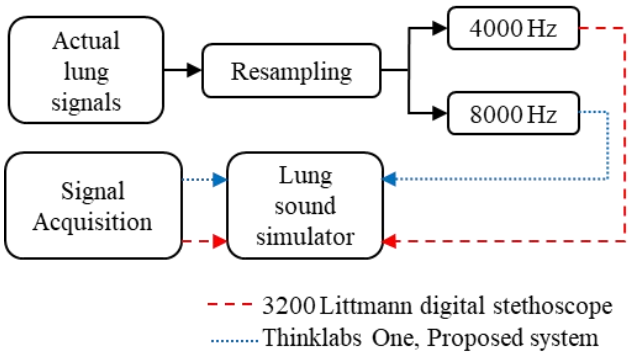


(b)

Fig. 11. Acquisition of lung signals. (a) Lung sound simulator for consistent and repeatable lung signal output. (b) The lung signals acquisition process.

### A. Acoustic Signals Acquisition and Setup

The following sub-sections describe the simulation and experimental setup for acquiring acoustic lung signals and lung imaging in this study.

#### 1) Acoustic Signals Acquisition

A lung sound signals simulator, as shown in Fig. 11, is preferable for repeatability when multiple devices and systems are required to evaluate the acquired signal in regard to noise performance [24]. A consistent comparison between multiple devices can be obtained when various variables in the actual signals recording, such as the patient's internal body movement sound and ambient noise profiles in the real world, are repeatable. Hence, 10 unhealthy lung sound signals with crackles and wheezing from patients diagnosed with asthma, or COPD, and 10 healthy lung signals of 15 seconds duration, recorded from the posterior of patients' chest, were selected from a respiratory database [28]. Then, each lung sound signal was independently played via a customized lung sound simulator at a sound amplitude output level similar to that of actual auscultation [9], [29].

The following steps were taken to shortlist the 20 lung signals (10 unhealthy, 10 healthy) from the large respiratory database [28], similar to the selection process utilized in the literature [9]. The lung signals collected from patients' posterior chests were first selected from the large respiratory database [28]. Next, the lung signals are separated into healthy and unhealthy lung sounds. Then, unhealthy lung sounds with unannotated adventitious lung sounds, such as crackles or wheezing from the clinicians or doctors, were omitted from the selection. Similarly, doctors or clinicians annotated adventitious lung sounds on healthy lung sounds were excluded. Lastly, the 10 unhealthy and 10 healthy lung signals were randomly selected from the remaining lung signals for the experimental study. Frequencies of interest of about 255 ± 60.53 Hz from the 10 healthy lung signals and 349 ± 52.39 Hz from the 10 unhealthy lung signals were detected using MATLAB R2023a frequency spectrum analysis, which also fall within the range reported in the literature [8], [30].

The customized lung sound simulator (see Fig. 11(a)) utilized a 15 mm thick silicone material (Baoblaze, USA) that closely resembled a human's skin, fat, and muscle layers and was placed on the top of an S1 Pro portable Bluetooth speaker system (BOSE, USA). The S1 Pro portable Bluetooth speaker system resembles a typical adult chest wall in terms of its overall size and has a frequency response (± 3 dB) ranging from 62 Hz to 17 kHz, which covers the acoustic frequencies of interest from 150 Hz to 1000 Hz [8]. Despite the large frequency response bandwidth, the S1 Pro portable Bluetooth speaker system has a flat frequency response ranging from 150 Hz to 1000 Hz [31]. The following setups were utilized to simulate the actual recording. The data recorded from the lung sound simulator during the signal acquisition study was conducted in a controlled acoustic environment with an average noise sound pressure level of 59 ± 0.54 dBA, which is comparable to a typical noisy clinical setting [32]. To maintain a consistent ambient noise power during each device assessment, the environmental noise was monitored using an omnidirectional sensitive and high SNR MP34DT04 MEMs microphone (STMicroelectronics, Switzerland). A JBL Xtreme

3 speaker, placed about 1 meter adjacent to the lung sound simulator, independently transmitted intensive care unit noise sounds randomly selected from a sound effect database at various levels [33]. The JBL Xtreme 3 speaker (Harman, USA) output was adjusted accordingly to control the true SNR, between -20 dB and 20 dB, with 5 dB intervals, similar to studies in [9], [29]. The setup allows us to test the suggested system directly against several other digital stethoscopes in a wide range of lung sound and background noise combinations.

The filtering and denoising capabilities of individual digital stethoscopes were considered to achieve reasonable signal acquisition performance comparison. Hence, the two digital stethoscopes' maximum bandwidth was utilized in this study. Littmann 3200 digital stethoscope filter option was set to "Extended mode," which amplifies sounds from 20 Hz to 2000 Hz, similar to a diaphragm, but provides more low-frequency response from 50 Hz to 500 Hz [12], [34]. The filtered lung sound signals are saved digitally in accompanying computer software. Thinklabs One digital stethoscope filter option was set to "Filter mode 5," wideband mode with a pass band between 20 Hz and 2000 Hz [35], and the digital lung sound signals are transmitted to the accompanying digital device for analysis. The bandwidth setting from the two digital stethoscopes covers the range of frequencies of interest (255 ± 60.53 Hz and 349 ± 52.39 Hz) of the selected lung signals for analysis.

The following steps (see Fig. 11(b)) were performed to obtain an equal total number of sample points between the broadcasted and recorded lung signals for valid signal analysis due to the differences in sample numbers and frequencies between the shortlisted lung sound for broadcasting and the three devices. The shortlisted lung signals, with a sampling frequency $F_S$ = 44100 Hz, were first resampled to match the default sampling frequency of the two digital stethoscopes and our proposed system before the start of the lung signals recording by the three devices. The shortlisted lung signals $F_S$ = 44100 Hz were resampled to 4000 Hz for 3200 Littmann digital stethoscope, and 8000 Hz for Thinklabs One digital stethoscope and our proposed system. The resampling process should not impact the overall broadcasting signals and can be justified as the shortlisted lung sounds are mostly low-frequency (255 ± 60.53 Hz and 349 ± 52.39 Hz) [8], [30]. The acquired signals from the three individual devices were compared to their respective resampled shortlisted lung sound signals for signal analysis.

2) *Acoustic Imaging Generation*

Various diameters of waterbag were positioned on the lung sound simulator's right middle, as illustrated in Fig. 12, to emulate the obstructed area in the airway [15], [16], [36] and to compare the nidus detection capability of the proposed system and the two digital stethoscopes through imaging translated from the captured lung signals. For repeatability and consistency in the acoustic imaging acquisition, the customized lung sound simulator played healthy lung sound from the respiratory database [28] and used a waterbag for airway obstruction as there are various recording locations from the respiratory database [28], such as the trachea, lateral, and anterior, and the exact unhealthy or obstructed lung sound position is unknown. The experiment is then repeated on a healthy volunteer with a waterbag attached to the posterior combined with the acoustic sensor design findings in [13] and [14] to locate the nidi length via imaging.

An array of MEMS microphone sensors was placed on the lung sound simulator without overlapping and with equal spacing to record signals, as shown in Fig. 1(a), while signals were taken independently (not simultaneous) by the two digital stethoscopes, in the same position as the MEMS microphone sensors, collecting an equal number of data points (sensor number), as presented in the example Fig. 12(a). The signals collected from the array of data points with our system and the two digital stethoscopes were then converted into acoustic image using the image algorithm in (2) and (3), similar to the literature [5]–[7]. Acoustic healthy reference images were generated [13], [14] individually with the recording of lung sounds from our system, and the two digital stethoscopes without the use of waterbag. E.g., Littmann 3200 has its independent, healthy image reference for comparison – obstructed acoustic image generated from Littmann 3200 is compared to healthy image generated from Littmann 3200, similarly for Thinklabs One and our proposed system. One representative healthy image is shown in Fig. 12(b) as the healthy lung image produced from the three devices look similar.

As 3M Littmann and Thinklabs One can only provide a single data point, the breathing phase was used to synchronize [23], [37] and form an array of lung sound signals and converts the lung sound signals into acoustic imaging (see Fig. 13),

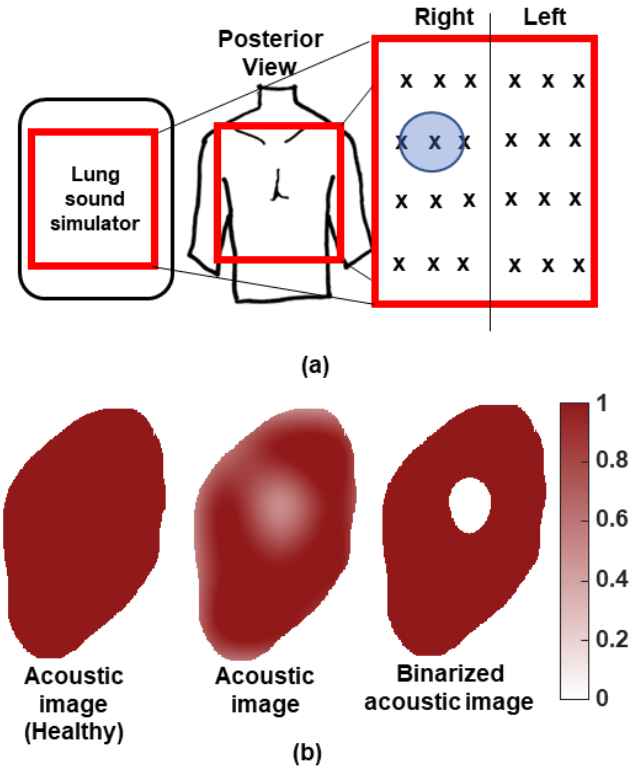


Fig. 12. The experimental and acquisition of acoustic imaging setup. (a) The schematic diagram of the experimental setup for capturing lung sound signals and nidus detection in the airways with waterbags. x denotes the positions of the acoustic sensors, such as MEMS and digital stethoscopes. The circular block presents an obstruction in the airways. (b) Binarized acoustic imaging for experimental results analysis.

similar to the typical acoustic imaging systems [15], [20], [21]. The respiratory signal synchronization technique from the literature [37] has demonstrated the detection of respiratory phases with an accuracy up to 0.2s in lung signals recordings containing minimal noise or significant noise interference. A 5th order FIR bandpass filter [37], consisting of a 1400 Hz low-pass cutoff frequency and a 150 Hz high-pass cutoff frequency is first applied to the digital stethoscope raw sound signals to improves detection of lower airway sounds by further eliminating aliasing, muscle, heart, and other low-frequency sounds. The identification of respiratory phases is based on the observation that louder sounds occur during transitions between phases. To detect these transitions more easily [37], an envelope of the signal is calculated using the Hilbert transform. The Hilbert transform generates a version of the input signal with a 90-degree phase shift, allowing computation of the signal's envelope while retaining the original time distribution. The identified analytic envelope local minima and maxima denote the signaling respiratory phase changes [37], as shown in Fig. 13.

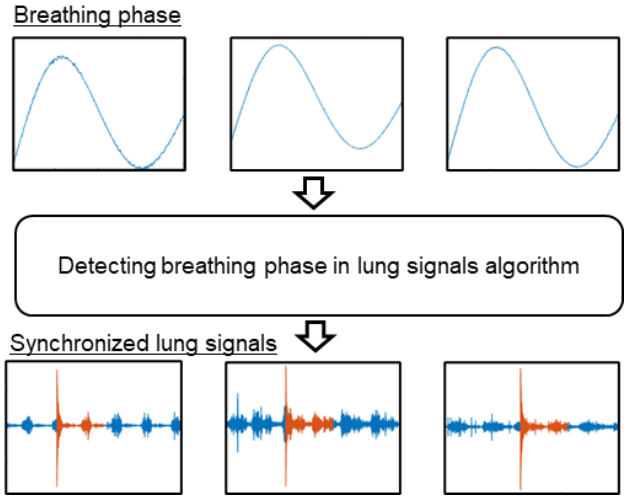


Fig. 13. Synchronizing an array of lung signals captured at different times via the breathing phase. Blue denotes the asynchronous lung signals captured due to single-point data. Red represents the synchronized lung signals via the breathing phase.

## B. Sensor Sensing Sensitivity, Signal Acquisition, and Identification of Nidi Performance Index

The following sub-section presents the performance metrics for sensor sensing sensitivity, acquired signal quality, and identifying nidi length through imaging translated from the acquired lung signals.

### 1) *Sensing Sensitivity Performance Index*

The devices and system signal pickup surface's sensitivity can be assessed by the sensor sensing sensitivity area. Fig. 14 depicts the setup for the sensitivity area measurement. In order to evaluate the sensitivity sensing area, our hardware system and the commercial digital stethoscopes were mounted directly on top of a 20 mm thick sound absorbing sheet (-25 dBA) with alternating 3-by-3 array of 6 mm hole diameter, similar to the sensor sensitivity study in [9].

Throughout the course of the sensor sensing sensitivity assessment, output signals $y_{ij}(n)$ are recorded for each position $i$ = [1, …, 9] and white noise $x_w(n)$ with a constant power is

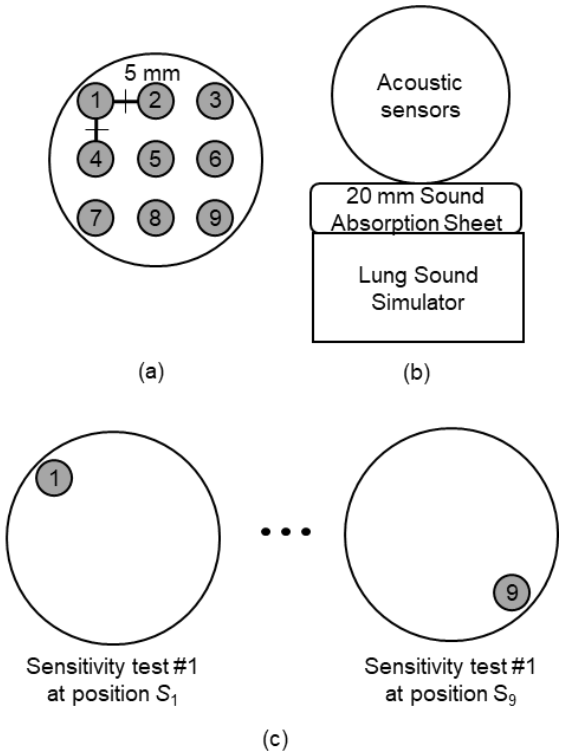


Fig. 14. The surface sensitivity performance setup with a single position capturing of acoustic signals at each interval, $S_1$, $S_2$, …, $S_9$. (a) Overview of sound absorption sheet with alternating 3-by-3 array. (b) The sensor sensing sensitivity test setup. (c) Example of alternating the sensitivity test.

consecutively played from each hole diameter of the position shown in Fig. 14 for $j$ = [1,.., 10] test.

The spectrum power of each output signal $y_{ij}(n)$ was calculated for frequencies between 100 Hz and 2000 Hz – the typical respiratory frequencies range, the two digital stethoscopes' maximum bandwidth, and the majority of the relevant lung sound signals are concentrated [9], [24]. The spectrum power from each output signal was compared to the center output signal $y_{5j}(n)$ position. The average spectrum power for each position $i$ is determined as,

$$\overline{S}_i = \frac{\left(\sum_{j=1}^{10} S_{ij}\right)}{10} \tag{6}$$

where the spectral power of the recorded signals $S_{ij}(n)$ is averaged across all $j$ tests. The acquired spectrum power from the 9 positions are then interpolated to achieve higher resolution for sensor sensing sensitivity analysis [9]. The logarithmic ratio $S = 10\log(\overline{S}_i/\overline{S}_5)$ is then used to compare the average power from the intermediate point $\overline{S}_5$ to each $\overline{S}_i$. The logarithmic ratio shows the effect of the position of input signals on the acquired signal [9].

### 2) *Signal Acquisition Performance Index*

RMSE and SNR were utilized as quantitative performance indices for indicating signal precision and noise robustness. RMSE is determined by employing the normalized digital amplitude of captured signal $r$, the normalized digital amplitude of actual signal $x$, and expressing the signals' digital amplitude differences in root mean squared sense as shown in (7), where the result closer to 0 indicates the better performing the device

is. SNR performance index can be expressed as (8) by finding the ratio and expressing the ratio using a logarithmic decibel scale between the normalized digital amplitude of captured signal $r$ and the normalized digital amplitude of noise $a_n$, where a larger value indicates better signal strength acquired in relation to noise.

$$\text{RMSE}=\sqrt{\frac{1}{N}\sum_{i=1}^{N}\left|x_i-r_i\right|^2}, \tag{7}$$

where $N$ is the total number of samples collected given as sampling frequency multiplied by a known time.

$$\text{SNR}=20\left[\log_{10}\left(\frac{r}{a_n}\right)\right], \tag{8}$$

where $a_n$ is the digital amplitude of the collected noise signals without the lung sound.

3) *Acoustic Imaging Performance Index*

The identification of nidi through imaging transmuted from acquired lung signals using (2) and (3) is compared across our system and the digital stethoscopes, where smaller differences in identified nidi when compared to the nidi true area indicate better accuracy. Through local first-order image statistics [38] around each pixel, the resulting unhealthy acoustic image area with airway blockage is converted into a binary image with a locally adaptive image threshold as 0s and all other values to 1s, as shown in Fig. 12. 1s represent healthy high-intensity data areas, whereas 0s represent obstructed low-intensity data areas in the binary image. The blockage (missing pixels) in the airway can be found by comparing the pixels between the healthy $\eta$ and unhealthy acoustic imaging areas $\mu$ using $(\eta - \mu)$. The nidus length $L_n = 2\sqrt{(\eta - \mu)/\pi}$ can then be calculated using the missing pixel's area [38].

## V. Results and Discussion

The sub-system performance, e.g., the acquired signal quality and the sensor sensing sensitivity between our system data acquisition and digital stethoscopes, are presented in Section V-A and Section V-B, respectively. The identification of nidi through translating the acquired signals into imaging is shown in Section V-C.

### A. Signal Accuracy and Noise Robustness

Fig. 15 displays the estimated SNR values (averaged across all trials, lung sounds, and noise signals) for each evaluated digital stethoscope along with our proposed system. Lower SNR values indicate deteriorated signal quality and substantial noise contamination. Conversely, higher SNR suggests low noise contamination and increased signal accuracy with the reference signal.

From Fig. 15, all three devices presented noise robustness in terms of the SNR of the input signal, similar to the trend in [9], particularly for digital stethoscopes, Littmann 3200, and Thinklabs One. The two digital stethoscopes and the proposed system feature advanced filtering to reduce interference, such as ambient noise and body movement from the lung sound signals [10]–[12]. An estimated SNR of about 25 dB was attained from the proposed system, and about 18 dB was attained by Littmann 3200 and Thinklabs One, regardless of the low- or high-SNR of input signals as presented in Fig. 15. Based on the overall measured SNR in Fig. 15, our hardware system exceeds the competition in terms of SNR in a noisy environment, due to the flexibility in implementing and optimizing the denoising algorithm [10] into our system architecture.

The mean RMSE results of the proposed system and the digital stethoscopes are presented in Fig. 16. RMSE measures the sensor's ability to acquire accurate signals and maintain major aspects of lung sound. Low values of the RMSE result indicate a low difference in signals captured and desired signals, whereas high values of the RMSE result show a certain level of error in the acquired signal. Overly suppressed filtered signal through the unoptimized and generic filter may result in high SNR, despite the filter introducing obvious distortions resulting in high RMSE results [10]. Hence, a balance between noise suppression (SNR) and signal accuracy (RMSE) is crucial for a lung sound acquisition system.

In contrast to the two digital stethoscopes, the proposed system can precisely capture the intended signal in terms of RMSE in a noisy environment, as shown in Fig. 16. The proposed system achieved better RMSE results by around 0.15

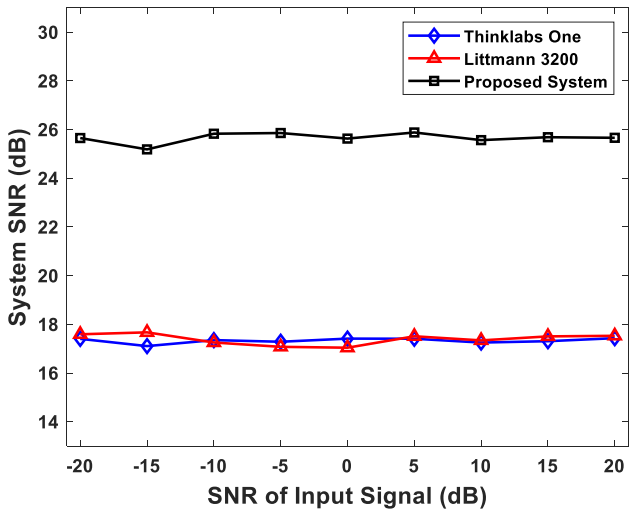


Fig. 15. The mean SNR performance between various sensors capturing lung sound signals in a noisy environment.

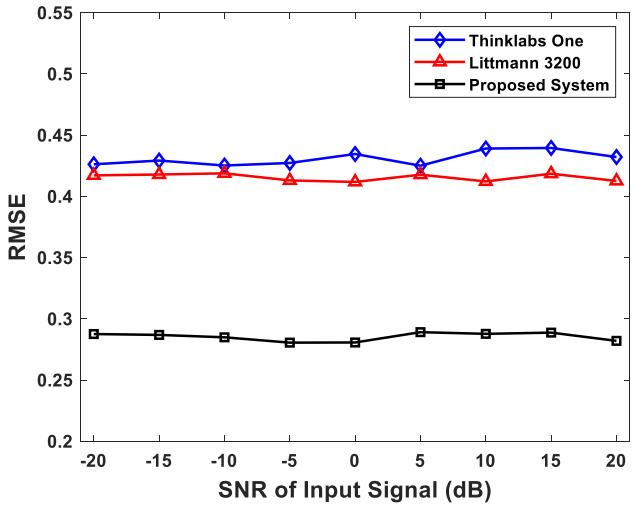


Fig. 16. The mean RMSE result between various sensors capturing lung sound signals in a noisy environment. As normalized digital amplitude was utilized in the signal analysis, the RMSE is unitless.

This article has been accepted for publication in IEEE Sensors Journal. This is the author's version which has not been fully edited and
content may change prior to final publication. Citation information: DOI 10.1109/JSEN.2023.3344136



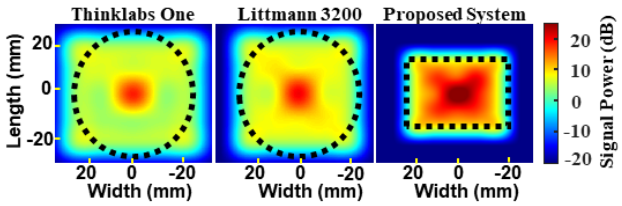


Fig. 17. Sensing sensitivity (dB) area compared to the power at the center position of various sensors, with the dashed line defining the sensor size. Thinklabs One digital stethoscope head (left), Littmann 3200 (center), and our hardware system (right).

compared to the digital stethoscopes with the implementation of the optimized denoising algorithm in [10]. The proposed system showed a high level of noise reduction while retaining the desired characteristics of the signal of interest, as demonstrated in Fig. 15 and Fig. 16.

With the addition of a denoising algorithm [10], as illustrated in Fig. 15 and Fig. 16, the proposed system has proven to be robust to noise and has captured more precise and desirable lung sound signals in terms of SNR and RMSE findings, respectively.

## B. Sensor Sensitivity

From Fig. 17, the proposed system surface sensitivity area was compared to the two commercial digital stethoscopes. Fig. 17 illustrates output spectral power as a function of the sound signal location in decibels with respect to the sensor's center position, and the spectrum power from the 9 positions are then interpolated [9] to achieve higher resolution for sensor sensing sensitivity analysis.

Digital stethoscopes lose their dynamic range substantially as the lung sound signals move outward and are most sensitive at the center of the stethoscope head, possibly due to the sensor sensing design [9], [11], [12]. The proposed system demonstrated a uniform sensing sensitivity across the sensing surface in terms of positional output spectral power to acquire lung sound.

Despite having a lower overall surface size than the two digital stethoscopes, the proposed system has a more uniform sensing sensitivity area of about >20 mm compared to the digital stethoscopes, which have uniform sensing areas of <10 mm. The proposed system provides a more uniform surface sensitivity in recording lung sound signals with a power spectral loss of approximately 5 dB (see Fig. 17) compared to the power spectral loss of about 10 dB from the two digital stethoscopes. The findings in Fig. 17 are consistent with the study in [9], especially with regard to positional output spectral trends in digital stethoscopes. Raw interpolated spectrum power data, i.e., no mask and outer boundary limit, was used in this section of the experiment, as the focus was on the sensitivity trend of the sensor surface, similar to the literature [9]. The sound absorption sheet utilized in the sensor sensitivity test is slightly larger (50 mm diameter) than our proposed system; hence, the complete absence of energy outside the sensing head area, as compared to the two digital stethoscopes sensing sensitivity mapping.

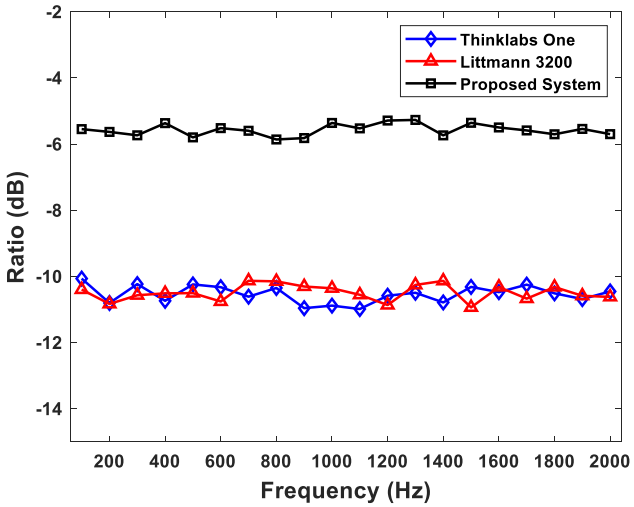


Fig. 18. The spectrum power ratio between the hardware system and the two digital stethoscopes from position $S_9$ in relation to the central position $S_5$, with 0 dB signifying equal signal power made from both positions.

Fig. 18 further highlights the performance variations in acquiring lung sound signals and the power loss at particular points. From Fig. 18, position $S_9$, far from the center $S_5$, was selected to demonstrate the power loss or sensitivity at a specific point on the proposed system and the digital stethoscopes. The proposed system maintains signal power at about 5 dB, relative to the center and across the frequencies of interest, in contrast to the two digital stethoscopes, which show a significant loss in power (down to 10 dB less) in Fig. 17 and Fig. 18. The results of this study on commercial digital stethoscopes support earlier findings that were presented in [9].

The sensitivity of the proposed system's sensor area makes it such that the exact location of the sensor on the body is not necessary to achieve the maximum amplitude. The other key benefit of the proposed system is that it enables better sound and data gathering for practice by healthcare practitioners with limited training.

## C. Acoustic Imaging

The proposed system and the digital stethoscopes are utilized for experimental study. With the typical adult chest surface area and the proposed sensor design, this study uses 12 and 16 sensor numbers [14] on a healthy volunteer with a waterbag attached to the posterior to record lung sounds. The waterbag's surface diameter of about 46 mm and 65 mm, the minimal detectable

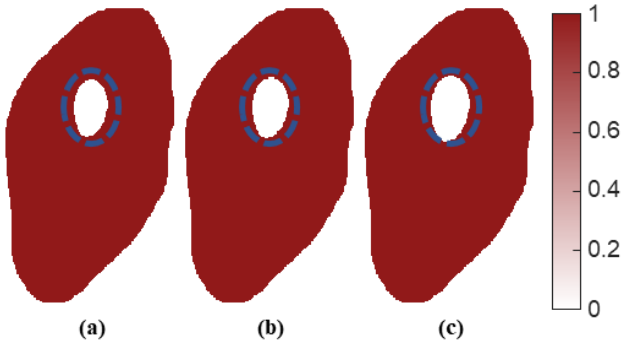


Fig. 19. Acoustic imaging of obstructed airway translated from acquired lung signals with 50 mm nidus length via the waterbag simulation, where the encircled dotted line indicates the actual waterbag size. (a) Thinklabs One, (b) Littmann 3200, and (c) the proposed system.

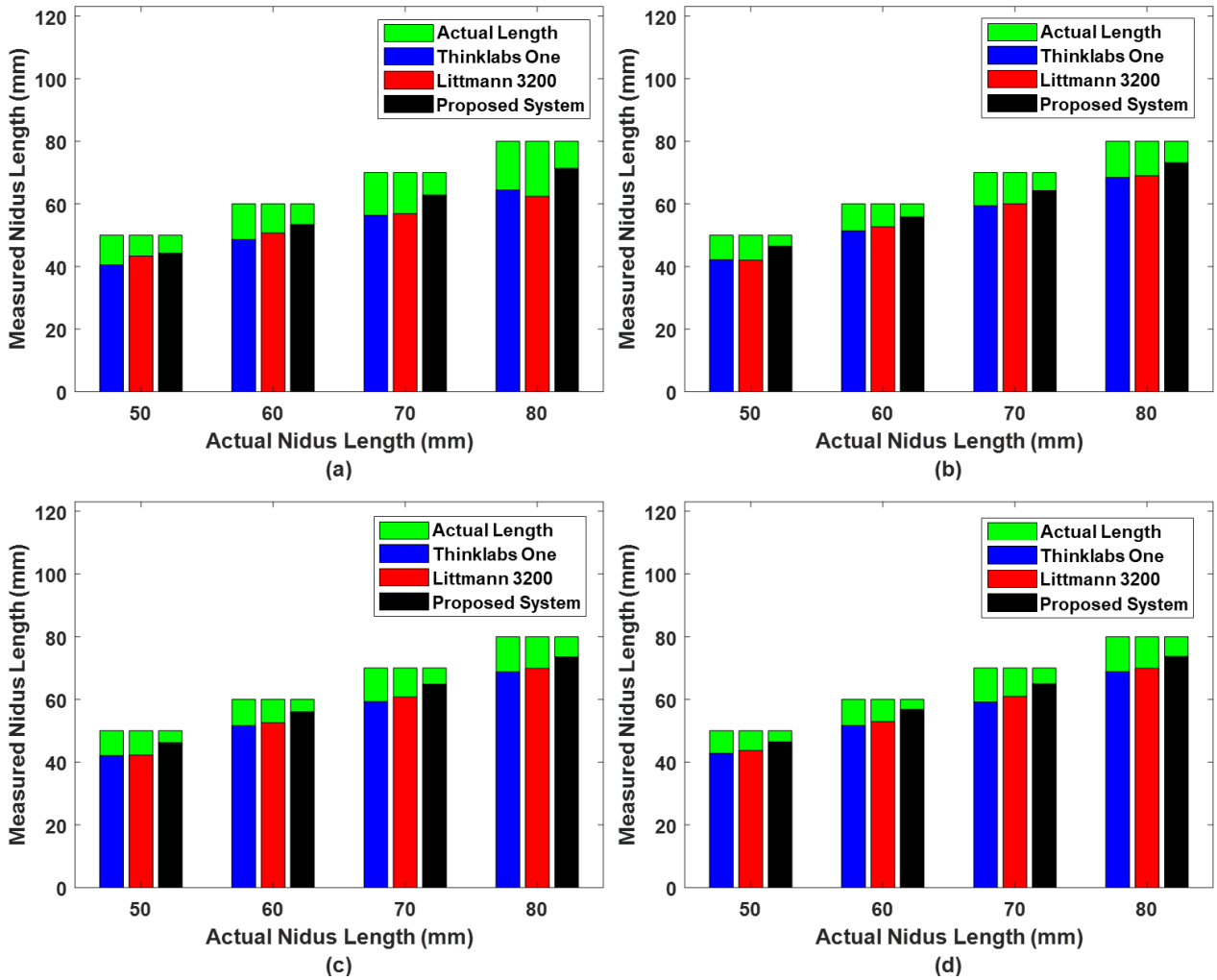


Fig. 20. Comparison between the proposed system and digital stethoscopes in detecting nidus through acoustic imaging with (a) 12, (b) 16, (c) 20, and (d) 24 sensors number.

nidus length from the modeling study in [14], was utilized.

Fig. 19 presented binarized acoustic imaging of obstructed airways translated from the captured lung signals with the proposed system and the commercial digital stethoscopes, simulated with a 50 mm waterbag. Standardized imaging algorithm presented in (2) and (3) was applied to the captured signals from our system and the commercial digital stethoscopes as the commercial digital stethoscopes do not produce imaging as an output. Fig. 20 demonstrated the accuracy of detecting various obstructed areas via acoustic imaging. Various waterbag diameter, ranging from 50 to 80 mm, was utilized to simulate the airway's obstructed area [15], [16], [36]. 50 to 80 mm waterbag diameters were selected due to the typical size that can be identified with acoustic imaging systems [14] employing the number of sensors from 12 to 24 [8], [15], [16], [21] and the typical adult lung size limit [39]. From Fig. 19 and Fig. 20, the proposed system outperforms the two digital stethoscopes in terms of the detected nidus length through acoustic imaging in (2) and (3) translated from lung signals, regardless of the number of sensors deployed. The proposed system achieved 91% accuracy in detecting the actual nidus length. In contrast, the two digital stethoscopes attained from 80 to 85% of accuracy in the detection of actual nidus length, potentially due to the acquired lung sound signals and the robustness to noise as the reliability of lung sound signals translates to the closeness of acoustic imaging [13]–[15], [21].

Fig. 21 demonstrated the nidus length detected with acoustic imaging on a healthy volunteer posterior with waterbag-simulated airway obstruction. The detected obstructed airway – minimum nidus length, is the shortest (higher resolution) with 16 sensors, whereas the minimum nidus length increases (lower resolution) with the decrease in sensor numbers, showing a similar trend compared to the modeling study in [14]. The results in Fig. 20 and Fig. 21 demonstrated the sensors number required to detect the minimum nidus length. E.g., 16 sensors can only detect the obstructed airway when the nidus length is greater than about 45 mm, while smaller obstructed airway with smaller nidus length of about 30 mm requires 35 sensors , as presented in Fig. 6 and in the literature [13], [14], and in line with the understanding that more sensors provide better resolution [5], [8], [17]. The results in Fig. 19–Fig. 21 demonstrated the potential of frequent lung health imaging through acoustic imaging converted from reliable captured lung signals, and the potential in enabling smarter high-frequency chest wall oscillation therapy by focusing on the obstructed lung region, reducing the therapy time.

A minimal difference of about 9% in the detected nidus length may be observed in Fig. 21 comparison between the

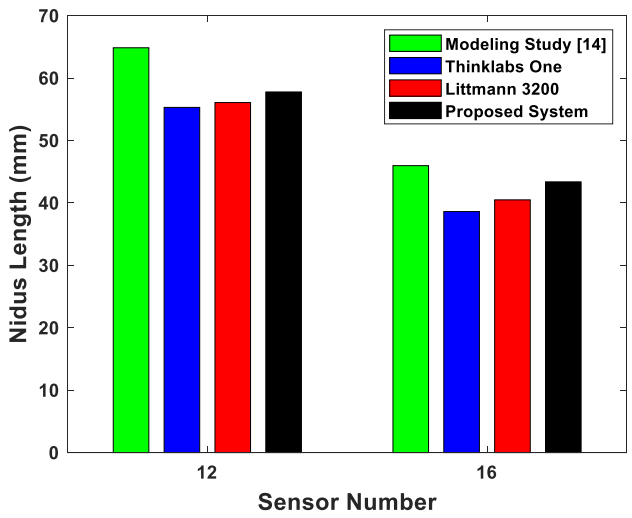


Fig. 21. The relation between the modeling study [14] and experimental validation on the minimal nidus length that can be observed at a fixed number of sensors on one side of the lung.

proposed system-generated experimental acoustic imaging and the modeling study in [14]. In contrast, detected nidi length differences of about 12 to 15% were observed between the digital stethoscopes and modeling study in [14]. The findings in Fig. 21 correspond to the earlier experimental results with the lung sound simulator, presented in Fig. 20, where the detected nidus length is about 91% (proposed system) and 80 to 85% (digital stethoscopes) within the actual nidus length. As this experimental validation comprises minimal ambient noise interference, a minimal difference is expected, given that the modeling study in [14] was based on an acoustic signal that was ideal and noise-free. Although an optimized denoising algorithm [10] was designed and integrated into the proposed system to reduce the interference noise pollution to the acoustic signals, minimal noise interference will still appear in the actual recording.

The minor discrepancies in the nidus length results in both the proposed system and digital stethoscopes, as presented in Fig. 20 and Fig. 21, between this experimental investigation and the modeling study in [14], may have been due to the airway models and the drawings employed. There are various airway models, including Horsfield, Weibel, and airway models based on animals. However, nidus detection was shown to be possible with acoustic imaging in this work and has corresponded with the modeling studies in [13] and [14]. Moreover, the nidus length is determined by the diameter of the obstructed lung area, which is assumed to be a perfect circle by the results in Fig. 21.

### *D. General Discussion*

Although the sensor sensitivity of the proposed system is neutral to the precise placement on the body, the minimum requirement of the array of acoustic sensor design is necessary for a reliable imaging output. E.g., detecting an 80 mm nidus length with a single sensor is not possible, while using minimally 12 sensors to detect an 80 mm nidus length with our sensor sensing area is possible [13], [14].

The separation of heart sounds from lung sounds was not taken into consideration in this study due to the emphasis on minimizing external interferences, such as environmental noises. The filter option was carefully adapted for the shortlisted digital stethoscopes in this study, highlighting lung signals' frequency of interest. The shortlisted lung sounds from the respiratory database, and recorded experimental lung sounds were signals from the volunteer's posterior to ensure that the heart sounds would be minimal and would not significantly interfere with the lung sounds.

There will likely be some variation in system performance, and should be taken into consideration due to several variables, such as physical product design, system architecture in terms of software and hardware acquisition, and signal filtering. The independent characteristics of the digital stethoscopes and the proposed system were used to calculate the quality performance outcomes in this study. E.g., no further signal processing was applied to the captured signals from the two digital stethoscopes as they have proprietary ambient noise reduction technology [11], [12] embedded in their digital stethoscopes. The proposed system uses adaptive noise suppression to remove ambient noise while preserving the lung sound signals as much as possible. The proposed system provides uniform sensitivity across the pickup surface, allowing reliable sound capture, while the two digital stethoscopes showed positional dependence in sensitivity, with about 10 dB drop in sensitivity towards the edges compared to the center, as shown in Fig. 17 and Fig. 18. The two digital stethoscope positional dependence in sensor sensitivity are likely due to the transducer design, which enhances the sensor overall aesthetic making it marketable but drops in sensor sensitivity, while our proposed system uses simple sensor casing design, maximizing the signal pick up area. Overall, the proposed system combines hardware redesign and signal processing to increase sensitivity, reduce noise, and preserve lung sounds of interest.

Although the experimental study interference was comparable to a typical noisy clinical environment, at an average sound pressure level of 59 ± 0.54 dBA, the current experimental study is performed at a well-controlled/simulated additive noise conditions and may have oversimplified environments in the actual busy clinical setting, where healthcare settings that are loud and rowdy result in unforeseen non-additive noise pollution.

The various lung sound acquisition systems and the proposed system should not be ranked in absolute terms based solely on signal and image accuracy, and noise robustness. The intention of this study is to benchmark our proposed system against established systems, proving the viability of utilizing acoustic imaging for frequent lung function assessment, converted from the captured lung signals. Similarly, the performance attained in this study should not be interpreted as showing how well a healthcare-trained professional can diagnose a patient using the proposed system without extended research. Moreover, the selections of digital stethoscopes in this study are not intended to be a representation of all digital stethoscopes available commercially, nor expressing opinions concerning their performances in noisy settings. What has been shown and validated in this study is each system's variability in response to acquiring signals with specific simulated external interference conditions.

Identifying early adventitious breath sounds through frequent monitoring of acoustics signals coming from the lungs with a wearable sensor device can offer critical lung function

information. For instance, intermittently turbulent airflow moving through the airways may indicate the existence of obstructive lung, where the signals are distinctive up to the 1000 Hz frequency range [8], [30]. Other than acoustic lung sound signals, breathing patterns and respiratory rate information with respect to lung signals can be utilized by clinicians and doctors to provide a more comprehensive diagnosis. E.g., the chest wall motion and breathing pattern-related macro vibrations also provide information about the patient's pulmonary health in addition to the high-frequency acoustic lung signals. A high respiratory rate (>30 breaths/min) is a common symptom of pneumonia and is a sensitive indicator of the illness. However, the patient's breathing patterns and respiratory rate was not considered in this study, as the study's main aim is to provide an early and accurate acoustic imaging assessment of lung function transmuted from lung signals rather than performing a diagnosis. The proposed system offers flexibility in acquiring lung sounds and then converts the lung signals into intuitive lung images to locate obstructed airways. Furthermore, substantial approaches to signal processing are needed to isolate the signal components and retrieve the pertinent data for diagnostic purposes, as the frequency ranges for specific breathing patterns and body movements overlap [30], [40]. In addition, the selection of the MEMS specification in this study was based on the CORSA — computerized respiratory sound analysis recommendations for sensor characteristics to detect human pulmonary sounds [8], [41]. Other MEMS, such as MEMS accelerometers [30], [40], MEMS piezoelectric resonant microphones [42], and strain gauges [43], have been utilized to capture breathing patterns and respiratory rate, a feature that is also currently unavailable in the digital stethoscope, to provide a comprehensive diagnosis with respect to lung signals. Readers who are interested in the precise diagnosis of respiratory disease can refer to [40], [42], [43] and the references therein for in-depth details on the fabrication of the various state-of-the-art MEMS.

## VI. Conclusion and Future Work

This study develops a wearable, extensible, and robust system of lung sound acquisition and acoustic imaging, which overcomes the limitations of current digital stethoscopes and produces more accurate acoustic images for continual lung function assessment. The proposed system is low-cost, ranging from USD 120 to 280, for a typical 12 to 24 acoustic sensors array [6], [7], [15], [17], [20], [21] recording lung sound simultaneously at different locations, as compared to digital stethoscopes [11], [12] USD 300, with only a single data point collection, excluding the cost of the computer for analysis. The objective criteria utilized in this study show how well the system preserves the characteristics of lung sound signals while minimizing external interferences. The proposed system outperforms the digital stethoscopes in terms of RMSE by around 0.15 and SNR by around 7 dB. Additionally, the proposed system has demonstrated a superior sensing sensitivity region regarding the recorded signal power spectrum compared to two well-known digital stethoscopes. The acoustic lung signals were converted into acoustic lung images for experimental investigation and analysis. The sensor distribution and acoustic imaging resolution modeling studies in [13] and [14], validated and supported the nidus detection results via acoustic imaging in the experimental study. Future research should examine the hardware system processing power in detail and consider real-world usage scenarios, such as respiratory conditions, to verify the system signal quality.

## References

[1] M. McIlwaine, J. Bradley, J. S. Elborn, and F. Moran, "Personalising airway clearance in chronic lung disease," *European Respiratory Review,* vol. 26, no. 143, p. 160086, 2017

[2] F. M. E. Franssen *et al.*, "Personalized medicine for patients with COPD: where are we?," *International journal of chronic obstructive pulmonary disease,* vol. 14, pp. 1465-1484, 2019

[3] C. Ohashi, S. Akiguchi, and M. Ohira, "Development of a Remote Health Monitoring System to Prevent Frailty in Elderly Home-Care Patients with COPD," *Sensors*, vol. 22, no. 7. doi: 10.3390/s22072670

[4] S. Janjua, D. Carter, C. J. D. Threapleton, S. Prigmore, and R. T. Disler, "Telehealth interventions: remote monitoring and consultations for people with chronic obstructive pulmonary disease (COPD)," *Cochrane Database of Systematic Reviews,* no. 7, 2021.

[5] R. P. Dellinger, J. E. Parrillo, A. Kushnir, M. Rossi, and I. Kushnir, "Dynamic visualization of lung sounds with a vibration response device: A case series," *Respiration,* vol. 75, no. 1, pp. 60-72, 2008.

[6] C. Shi *et al.*, "Assessment of Regional Ventilation Distribution: Comparison of Vibration Response Imaging (VRI) with Electrical Impedance Tomography (EIT)," *PLOS ONE,* vol. 9, no. 1, p. e86638, 2014.

[7] C.-S. Lee, M. Li, Y. Lou, Q. H. Abbasi, and M. A. Imran, "Acoustic Lung Imaging Utilized in Continual Assessment of Patients with Obstructed Airway: A Systematic Review," *Sensors*, vol. 23, no. 13, p. 6222, Jul. 2023.

[8] A. Rao, E. Huynh, T. J. Royston, A. Kornblith, and S. Roy, "Acoustic Methods for Pulmonary Diagnosis," *IEEE Reviews in Biomedical Engineering,* vol. 12, pp. 221-239, 2019.

[9] I. McLane, D. Emmanouilidou, J. E. West, and M. Elhilali, "Design and Comparative Performance of a Robust Lung Auscultation System for Noisy Clinical Settings," *IEEE Journal of Biomedical and Health Informatics,* vol. 25, no. 7, pp. 2583-2594, 2021.

[10] C. S. Lee, M. Li, Y. Lou, and R. Dahiya, "Restoration of Lung Sound Signals Using a Hybrid Wavelet-Based Approach," *IEEE Sensors Journal,* vol. 22, no. 20, pp. 19700-19712, 2022.

N. R. Council, *Health risks from exposure to low levels of ionizing radiation: BEIR VII phase 2*. National Academies Press, 2006.

[11] *ThinklabsOne*. Accessed on Oct. 13, 2022. [Online]. Available: https://www.thinklabs.com/

[12] *3M Littmann Electronic Stethoscope Model 3200*. Accessed on Oct. 13, 2022. [Online]. Available: https://www.3m.com.sg/3M/en_SG/p/d/v000179163/

[13] C. S. Lee, M. Li, Y. Lou and R. Dahiya, "Modeling and Simulation of Pulmonary Acoustic Signal and Imaging for Lung Function Assessment," *2023 IEEE International Conference on Consumer Electronics (ICCE)*, Las Vegas, NV, USA, 2023, pp. 01-06.

[14] C. S. Lee, Y. Lou, M. Li, Q. H. Abbasi and M. Imran, "Locating Nidi for High-Frequency Chest Wall Oscillation Smart Therapy via Acoustic Imaging of Lung Airways as a Spatial Network," in *IEEE Access*, 2023. doi: 10.1109/ACCESS.2023.3317443.

[15] M. Kompis, H. Pasterkamp, and G. R. Wodicka, "Acoustic Imaging of the Human Chest," *Chest,* vol. 120, no. 4, pp. 1309-1321, 2001.

[16] S. Charleston-Villalobos, R. Gonzalez-Camarena, G. Chi-Lem, and T. Aljama-Corrales, "Acoustic Thoracic Images for Transmitted Glottal Sounds," in *2007 29th Annual International Conference of the*

*IEEE Engineering in Medicine and Biology Society*, 2007, pp. 3481-3484.
[17] S. Charleston-Villalobos, S. Cortés-Rubiano, R. González-Camerena, G. Chi-Lem, and T. Aljama-Corrales, "Respiratory acoustic thoracic imaging (RATHI): Assessing deterministic interpolation techniques," *Medical and Biological Engineering and Computing,* vol. 42, no. 5, pp. 618-626, 2004.
[18] J. W. Szem, L. J. Hydo, E. Fischer, S. Kapur, J. Klemperer, and P. S. Barie, "High-risk intrahospital transport of critically ill patients: safety and outcome of the necessary "road trip"," *Crit Care Med,* vol. 23, no. 10, pp. 1660-6, 1995.
[19] U. Beckmann, D. M. Gillies, S. M. Berenholtz, A. W. Wu, and P. Pronovost, "Incidents relating to the intra-hospital transfer of critically ill patients. An analysis of the reports submitted to the Australian Incident Monitoring Study in Intensive Care," *Intensive Care Med,* vol. 30, no. 8, pp. 1579-85, Aug 2004.
[20] S. Lev *et al.*, "Computerized Lung Acoustic Monitoring Can Help to Differentiate between Various Chest Radiographic Densities in Critically Ill Patients," *Respiration,* vol. 80, no. 6, pp. 509-516, 2010.
[21] D. Bing, K. Jian, S. Long-feng, T. Wei, and Z. Hong-wen, "Vibration response imaging: a novel noninvasive tool for evaluating the initial therapeutic effect of noninvasive positive pressure ventilation in patients with acute exacerbation of chronic obstructive pulmonary disease," *Respiratory Research,* vol. 13, no. 1, p. 65, 2012.
[22] C. TDK Group. *ICS-52000*. Accessed on Jan 30, 2023. [Online]. Available: https://invensense.tdk.com/products/ics-52000/
[23] E. Messner, M. Hagmüller, P. Swatek, and F. Pernkopf, "A Robust Multichannel Lung Sound Recording Device," presented at the Proceedings of the International Joint Conference on Biomedical Engineering Systems and Technologies, Rome, Italy, 2016.
[24] F. Meng, Y. Wang, Y. Shi, and H. Zhao, "A kind of integrated serial algorithms for noise reduction and characteristics expanding in respiratory sound," *International Journal of Biological Sciences,* Research Paper vol. 15, no. 9, pp. 1921-1932, 2019.
[25] M. Nissan and N. Gavriely, "A microcomputer based lung sounds analysis," *Computer Methods and Programs in Biomedicine,* vol. 40, no. 1, pp. 7-13, 1993.
[26] PJRC. *Teensy® 3.6 Development Board*. Accessed on Jan 30, 2023. [Online]. Available: https://www.pjrc.com/store/teensy36.html
[27] D. Singh, B. K. Singh, and A. K. Behera, "Comparative analysis of Lung sound denoising technique," in *2020 First International Conference on Power, Control and Computing Technologies (ICPC2T)*, 2020, pp. 406-410.
[28] B. M. Rocha *et al.*, "An open access database for the evaluation of respiratory sound classification algorithms," *Physiological Measurement,* vol. 40, no. 3, p. 035001, 2019.
[29] S. S. Kraman, "Transmission of lung sounds through light clothing," *Respiration*, vol. 75, no. 1, pp. 85-88, 2008.
[30] P. Gupta, H. Wen, L. Di Francesco, and F. Ayazi, "Detection of pathological mechano-acoustic signatures using precision accelerometer contact microphones in patients with pulmonary disorders," *Scientific Reports*, vol. 11, no. 1, p. 13427, 2021.
[31] *Frequency Response Graph (Bose S1 Pro System)*. Accessed on Jul. 09, 2023. [Online]. Available: https://www.rtings.com/speaker/0-8/graph#6982/4559
[32] J. L. Darbyshire, M. Müller-Trapet, J. Cheer, F. M. Fazi, and J. D. Young, "Mapping sources of noise in an intensive care unit," *Anaesthesia,* vol. 74, no. 8, pp. 1018-1025, 2019.
[33] British Broadcasting Corporation (BBC). Sound Effects. Accessed on Jun. 20, 2023. [Online]. Available: https://sound-effects.bbcrewind.co.uk/search?q=Intensive%20care%20unit
[34] *3M Littmann electronic stethoscope model 3200 (p.p. 7)*. Accessed on Jul. 7, 2023. [Online]. Available: https://multimedia.3m.com/mws/media/594115O/3m-littmann-electronic-stethoscope-model-3200-user-manual.pdf
[35] *The audio filter in your One*. Accessed on Jul. 7, 2023. [Online]. Available: http://thinklabsone.com/downloads/Stethoscope_Filters.pdf
[36] S. M. A. Salehin and T. D. Abhayapala, "Lung sound localization using array of acoustic sensors," in *2008 2nd International Conference on Signal Processing and Communication Systems*, 2008, pp. 1-5.
[37] D. Skalicky, V. Koucky, D. Hadraba, M. Viteznik, M. Dub, and F. Lopot, "Detection of respiratory phases in a breath sound and their subsequent utilization in a diagnosis," *Applied Sciences*, vol. 11, no. 14, 2021.
[38] D. Bradley and G. Roth, "Adaptive Thresholding using the Integral Image," *Journal of Graphics Tools,* vol. 12, no. 2, pp. 13-21, 2007.
[39] G. H. Kramer, K. Capello, B. Bearrs, A. Lauzon, and L. Normandeau, "Linear dimensions and volumes of human lungs obtained from CT images," *Health Physics,* vol. 102, no. 4, 2012.
[40] P. Gupta, M. J. Moghimi, Y. Jeong, D. Gupta, O. T. Inan, and F. Ayazi, "Precision wearable accelerometer contact microphones for longitudinal monitoring of mechano-acoustic cardiopulmonary signals," *npj Digital Medicine*, vol. 3, no. 1, p. 19, 2020.
[41] L. Vannuccini et al., "Capturing and preprocessing of respiratory sounds," *Eur Respir Rev*, vol. 10, pp. 616-620, 2000.
[42] H. Liu et al., "MEMS piezoelectric resonant microphone array for lung sound classification," *Journal of Micromechanics and Microengineering*, vol. 33, no. 4, p. 044003, 2023.
[43] M. Chu et al., "Respiration rate and volume measurements using wearable strain sensors," *npj Digital Medicine*, vol. 2, no. 1, p. 8, 2019.

**Chang Sheng Lee** received the B.Eng. degree in mechatronics engineering from University of Glasgow, United Kingdom, in 2013 and the M.Sc. degree in mechanical engineering from National University of Singapore, Singapore, in 2016. He is currently pursuing the Ph.D. degree in electrical engineering at University of Glasgow, United Kingdom. He is currently in the Global Technology Integration department with Hill-Rom Services Pte Ltd, Singapore as a Research Engineer. His Ph.D. work is focused on the development of sensing technologies and system for lung health assessment.

**Minghui Li** (SM'22) received the B.Eng. and M.Eng. degrees from Xidian University, Xi'an, China, in 1994 and 1999, respectively, and the Ph.D. degree from Nanyang Technological University (NTU), Singapore, in 2004, all in electrical engineering. From 1994 to 1996, he was a Faculty Member with the School of Electronic Engineering, Xidian University. From 1999 to 2000, he was a Research Engineer with SIEMENS (China) Co., Ltd., Beijing, China. From 2003 to 2008, he was first with the School of Electrical and Electronic Engineering and then with the Intelligent Systems Center, Nanyang Technological University (NTU) as a Research Fellow. From 2008 to 2013, he was a Lecturer with the Department of Electronic and Electrical Engineering, University of Strathclyde, U.K. He joined the School of Engineering, University of Glasgow, U.K., as an Associate Professor in August 2013. His research interests include phased array systems, array design and processing, direction-of-arrival estimation, adaptive and arbitrary beamforming, spatial-temporal processing and coding, smart antennas, MIMO, evolutionary computation, wireless sensor networks, and coded ultrasound, with application to modern radar, underwater sonar, medical diagnosis, non-destructive evaluation, and wireless communications.

**Yaolong Lou** (SM'11) received the B.Eng. and M.Eng. degrees from Harbin Institute of Technology, Harbin, China, in 1985 and 1988, respectively, and the *Dr.-Ing.* degree from The University of Wuppertal, Wuppertal, Germany, in 1996, all in electrical engineering. From 1997 to 1998, he was a Postdoctoral Fellow with the National University of Singapore. From 1999 to 2003, he was first a Senior Engineer then a Principal Engineer with Singapore Research Laboratory of Sony Electronics. From 2003 to 2005, he was a Chief Engineer with Philips Electronics in Singapore. From 2006 to 2007, he was a Staff Engineer with Seagate Technology International in Singapore. Since 2007, he has been with Welch Allyn later Hill-Rom in Singapore as Principal Engineer, R&D Manager and Senior Manager for Innovation in Global Technology Integration department. Dr. Lou's areas of interest include small and special electrical machines and their controls, motion control systems, intelligent control with neural networks; system analysis, modeling, and simulation; as well as medical devices and image processing for cardiovascular and respiratory systems and vision care systems.

**Qammer H. Abbasi** (SMIEEE, MIET, FRET, FRSA), Dr Abbasi is a Reader with the James Watt School of Engineering, University of Glasgow, U.K., deputy head for Communication Sensing and Imaging group. He has published 350+ leading international technical journal and peer reviewed conference papers and 10 books and received several recognitions for his research including URSI 2019 Young Scientist Awards, UK exceptional talent endorsement by Royal Academy of Engineering, Sensor 2021 Young Scientist Award, National talent pool award by Pakistan, International Young Scientist Award by NSFC China, National interest waiver by USA and 8 best paper awards. He is a committee member for IEEE APS Young professional, Sub-committee chair for IEEE YP Ambassador program, IEEE 1906.1.1 standard on nano communication, IEEE APS/SC WG P145, IET Antenna Propagation and healthcare network

**Muhammad Imran (**Fellow, IEEE) Fellow IET, Senior Member IEEE, Senior Fellow HEA is Dean University of Glasgow UESTC and a Professor of Wireless Communication Systems with research interests in self organized networks, wireless networked control systems, internet of things (IoT) and the wireless sensor systems. He heads the Communications, Sensing and Imaging (CSI) research group at University of Glasgow and is the Director of Glasgow-UESTC Centre for Educational Development and Innovation. He is an Affiliate Professor at the University of Oklahoma, USA and a visiting Professor at 5G Innovation Centre, University of Surrey, UK. He has over 20 years of combined academic and industry experience with several leading roles in multi-million pounds funded projects. He has filed 15 patents; has authored/co-authored over 400 journal and conference publications; has edited 7 books and authored more than 30 book chapters; has successfully supervised over 40 postgraduate students at Doctoral level. He has been a consultant to international projects and local companies in the area of self-organized networks.